Elastic and inelastic scattering of polarized ^{6}Li by ^{26}Mg at 60 MeV

R. P. Ward* and N. M. Clarke*
Wheatstone Laboratory, King's College London, Strand, London WC2R 2LS, England
and School of Physics and Space Research, University of Birmingham, Edgbaston, Birmingham B15 2TT, England

K. I. Pearce† and C. N. Pinder‡
Wheatstone Laboratory, King's College London, Strand, London WC2R 2LS, England

C. O. Blyth, H. D. Choi,§ P. R. Dee, S. Roman, and G. Tungate
School of Physics and Space Research, University of Birmingham, Edgbaston, Birmingham B15 2TT, England

N. J. Davis
Department of Physics, University of Edinburgh, Mayfield Road, Edinburgh EH9 3JZ, Scotland
(Received 15 December 1993)

Angular distributions of differential cross section and vector analyzing power have been measured for the elastic and inelastic scattering of polarized ^{6}Li by ^{26}Mg at 60 MeV bombarding energy. The data have been compared with the results of coupled-channels calculations using phenomenological potentials and coupling strengths derived from inelastic scattering cross-section data and $B(E2)$ values. The data are reproduced by calculations including couplings between the ground and excited states of the projectile.

PACS number(s): 25.10.+s, 24.70.+s, 24.10.Eq, 27.30.+t

I. INTRODUCTION

Analyzing powers for polarized heavy ion scattering are known to be strongly influenced by inelastic and reorientation couplings in the projectile. A thorough review of such studies has been given by Fick *et al.* [1]. Analyzing powers for the elastic and inelastic scattering of polarized ^{6}Li from ^{26}Mg at 44 MeV bombarding energy were measured by Rusek *et al.* [2], who then performed a coupled-channels (CC) analysis. The data obtained by Rusek *et al.* were reanalyzed by Hirabayashi and Sakuragi, who concluded that vector analyzing powers for this system were largely the result of a dynamic spin-orbit potential generated by couplings between the ground and excited states of the projectile [3]. To fully reproduce the 44 MeV data Hirabayashi and Sakuragi found it necessary to include couplings between the 1^+ ground and the 3^+ (2.18 MeV), 2^+ (4.31 MeV), and 1^+ (5.65 MeV) resonant excited states of ^{6}Li, which form a $T = 0$ triplet above the threshold for $^6\text{Li} \rightarrow \alpha + \text{d}$ breakup at 1.47 MeV. However, Reber *et al.* [4] reported that calculations coupling the $1^+_{\text{g.s.}}$, 3^+, and 2^+ states in ^{6}Li yielded a description of data for $^6\vec{\text{Li}} + ^9$Be elastic scattering inferior to that obtained from calculations coupling just the $1^+_{\text{g.s.}}$ and 3^+ states. Thus, the role of projectile excitation couplings in $^6\vec{\text{Li}}$ scattering is by no means clear.

The role of nonresonant continuum states in the elastic scattering of polarized ^{6}Li is unclear at the moment. Hirabayashi [5] performed extensive continuum-discretized coupled-channels (CDCC) calculations for the elastic scattering of $^6\vec{\text{Li}}$ by ^{26}Mg at a bombarding energy of 99 MeV and demonstrated that the effects of the nonresonant states on the predicted analyzing powers were as profound as the effects of the resonant states. However, when the technique was applied to 44 MeV scattering and the results compared with the data of Rusek *et al.* [2], the vector analyzing power data were poorly described, although the descriptions of the differential cross section and tensor analyzing power data were good.

The importance of the static spin-orbit potential in polarized ^{6}Li scattering is also unclear at the moment. There is evidence to suggest that while the static spin-orbit potential is unimportant in the description of vector analyzing powers for elastic scattering, large vector analyzing powers for inelastic scattering populating excited states in the target nucleus can only be described when a static spin-orbit potential is used [4,6]. However, Rusek *et al.* failed to reproduce their vector analyzing power data for inelastic scattering even with the inclusion of a static spin-orbit potential [2]. The calculations of Hirabayashi and Sakuragi [3] and Hirabayashi [5] did

*Present address: School of Physics and Space Research, University of Birmingham, Edgbaston, Birmingham B15 2TT, England.
†Present address: Nuclear Electric, Berkeley Technology Centre, Berkeley, Gloucestershire GL13 9PB, England.
‡Present address: Particle Physics Department, Rutherford Appleton Laboratory, Chilton, Didcot, Oxfordshire OX11 0QX, England.
§Present address: Department of Physics, Kyungpook University, Taegu 702–701, Korea (South).

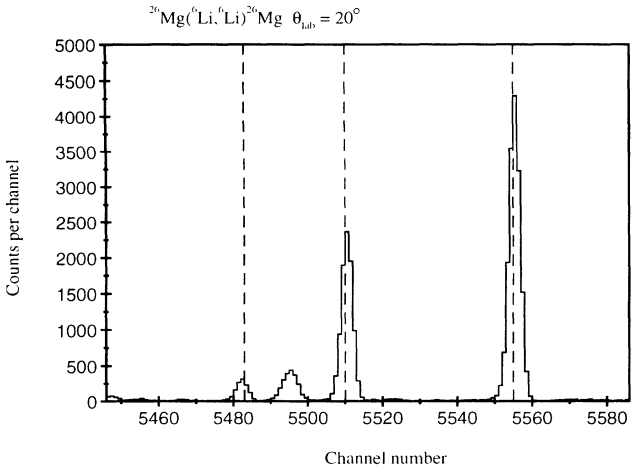

FIG. 1. Sample ^{6}Li spectrum. The dashed lines indicate, from right to left, states in ^{26}Mg at excitation energies of 0, 1.809, and 2.938 MeV, respectively. The other peak visible in this spectrum is due to ^{16}O contamination of the target.

not include target excitation. A recent study by Reber *et al.* [7] concluded that much of the structure observed in analyzing power data for $^{6}\vec{\text{Li}} + ^{12}$C elastic and inelastic scattering can be explained using static spin-orbit and tensor potentials alone.

The present work reports new data for the elastic and inelastic scattering of vector-polarized ^{6}Li by ^{26}Mg at 60 MeV bombarding energy and describes an analysis of those data with reference to the resonant excited states of ^{6}Li. CDCC calculations of the type published by Hirabayashi [5] lie beyond the resources of the authors of the present work.

II. EXPERIMENT

The experiment was performed using the polarized heavy ion source [8] and tandem Van de Graaff accelerator [9] at the Nuclear Structure Facility, SERC Daresbury Laboratory. The elastic and inelastic scattering data analyzed in the present work were obtained simultaneously with the charge-exchange data published by Ward

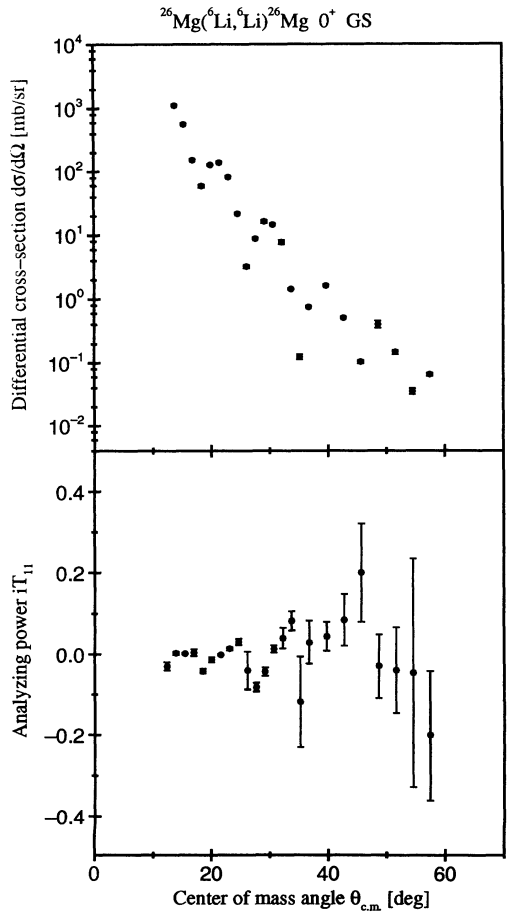

FIG. 2. Angular distributions of differential cross section and vector analyzing power for the elastic scattering of ^{6}Li by ^{26}Mg at 60 MeV.

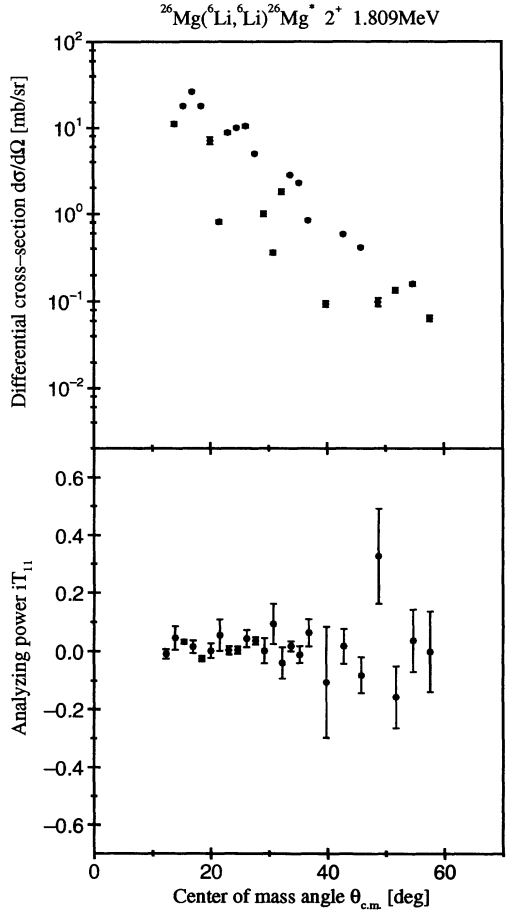

FIG. 3. Angular distributions of differential cross section and vector analyzing power for the inelastic scattering of ^{6}Li by ^{26}Mg at 60 MeV, populating the 2^{+} (1.809 MeV) state in ^{26}Mg.

et al. [10], who gave a full description of the data acquisition. A sample ^{6}Li spectrum is shown in Fig. 1. The present work reports the analysis of angular distributions of differential cross section and vector analyzing power for the 0^+ ground and 2^+ (1.809 MeV) states in ^{26}Mg. The closure of the Nuclear Structure Facility prevented the measurement of the analyzing powers T_{20}, T_{22}, and T_{21}. The Madison Convention [11] is used throughout the present work.

The measured data for elastic and inelastic scattering are shown in Figs. 2 and 3, respectively, to facilitate comparison with the data obtained by Rusek *et al.* [2]. It should be noted that the vector analyzing power data of Rusek *et al.* were presented as $^TT_{10}(\theta)$ rather than $iT_{11}(\theta)$, where $^TT_{10}(\theta) = \sqrt{2}iT_{11}(\theta)$. The present elastic scattering differential cross-section data have maxima at approximately 20°, 30°, 40°, and 50° center of mass which seem analogous to the maxima near 25°, 35°, 45°, and 58° center of mass in the 44 MeV data reported by Rusek *et al.* Furthermore, the value of $iT_{11} \sim +0.1$ seen in the present data near 35° center of mass is analogous with an observation near 40° center of mass in the 44 MeV vector analyzing power data of Rusek *et al.* Thus, the present elastic scattering data and the data of Rusek *et al.* appear to have many common features.

The present inelastic scattering differential cross-section data exhibit maxima near 25°, 35°, and 45° center of mass. Rusek *et al.* [2] published differential cross-section data for this state in the angular range $30° < \theta_{\text{c.m.}} < 80°$, with maxima near 32°, 42°, and 52° center of mass. Thus, the two differential cross-section data sets seem to agree well over the angular range common to both. The present vector analyzing power data for this state are near zero for $\theta_{\text{c.m.}} < 40°$ and mainly negative for larger angles. However, the vector analyzing power data of Rusek *et al.* are positive for $\theta_{\text{c.m.}} > 40°$, indicating some difference between the data sets. It should be noted though that the data of Rusek *et al.* are statistically far superior to the present data in this angular region.

III. ANALYSIS

A. Optical potential

In much of the work described in this paper, the interaction between the projectile and target nuclei was described by the spherically symmetric optical potential $U(r)$ given by

$$U(r) = V_c(r) - V_0 f(x_0) - i\left(W_s f(x_s) - 4a_d W_d \frac{d}{dr} f(x_d)\right) + \frac{V_{\text{s.o.}}}{r}\left(\frac{\hbar}{m_\pi c}\right)^2 \frac{d}{dr} f(x_{\text{s.o.}})\mathbf{l}\cdot\mathbf{s} \quad (1)$$

where $\mathbf{l}$ and $\mathbf{s}$ are the orbital angular momentum and intrinsic spin operators, respectively. The potential form-factors $f(x_n)$ have the Woods-Saxon shape given by

$$f(x_n) = (e^{x_n} + 1)^{-1} \quad (2)$$

and

$$x_n = \frac{r - r_n A^{1/3}}{a_n} \quad (3)$$

where r_n and a_n are the reduced radius and diffuseness of the potential, respectively. V_c is the Coulomb potential due to a sphere of 1.25 fm reduced radius and A is the mass number of the target nucleus.

The starting point of the analysis was a search to the differential cross-section data for elastic scattering using the optical model search code HI-OPTIM [12]. The starting parameters were those reported by Fulmer *et al.* for the elastic scattering of 88 MeV ^{6}Li from ^{26}Mg [13]. These parameters are shown as set 1 in Table I; $V_{\text{s.o.}}$ was kept equal to zero during these searches. The parameters derived from the search are set 2 in Table I. The differential cross-section data could not be described acceptably using a Woods-Saxon derivative form for the

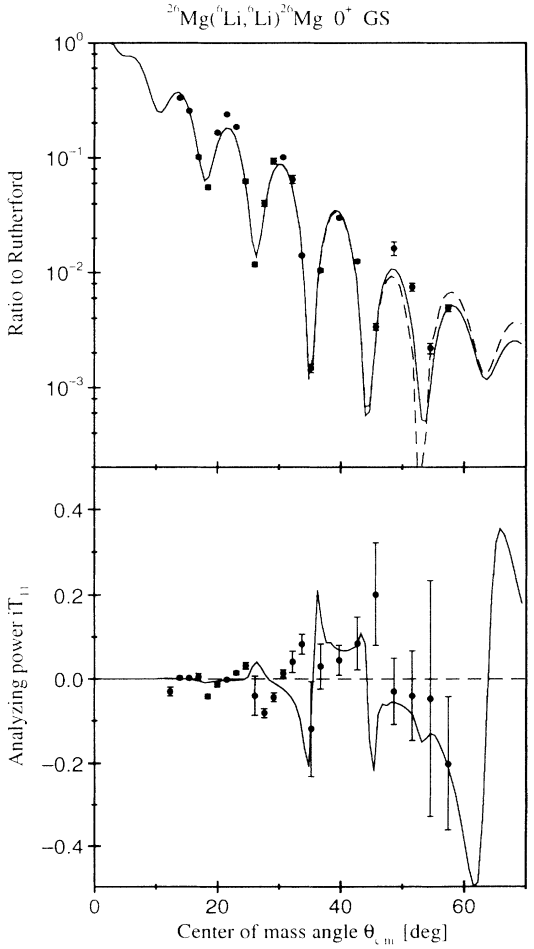

FIG. 4. Optical model calculations for the elastic scattering of ^{6}Li from ^{26}Mg at 60 MeV. The solid line includes a static spin-orbit potential, while the dashed line neglects the static spin-orbit potential.

TABLE I. Optical model parameters for the elastic scattering of 60 MeV ^{6}Li by ^{26}Mg. The Coulomb radius was assumed to be $r_c = 1.25$ fm in all cases. Potential depths are in MeV and geometric parameters are in fm.

Set	V_0	r_0	a_0	W_s	r_s	a_s	Reference
1	158.7	1.148	0.859	24.1	1.810	0.792	[13]
2	166.4	1.150	0.847	15.7	2.005	0.709	This work

TABLE II. Deformed optical model parameters derived from the CC analysis of differential cross-section data for elastic and inelastic scattering. Potential depths are in MeV and geometric parameters are in fm.

Set	V_0	r_0	a_0	W_s	r_s	a_s	r_c	β_2
1	166.430	1.150	0.847	15.663	2.010	0.727	1.250	± 0.300
2	189.210	1.150	0.833	16.604	2.010	0.619	1.250	$+0.236$
3	182.797	1.150	0.843	16.305	2.010	0.620	1.250	-0.277

imaginary potential. A search was performed to locate other discrete ambiguity families, but none were found, in agreement with the findings of Cook *et al.* [14].

Optical model predictions for the differential cross section and vector analyzing power corresponding to parameter set 2 in Table I are shown as dashed lines in Fig. 4. The solid lines in Fig. 4 are optical model predictions with a static spin orbit in addition to set 2 in Table I. This static spin-orbit potential was derived by Mairle *et al.* [15] from polarized deuteron scattering by ^{28}Si at 52 MeV, having $V_{s.o.} = 4.94$ MeV, $r_{s.o.} = 1.20$ fm, and $a_{s.o.} = 0.40$ fm, and was used in the folding-model calculations of previous analyses of polarized ^{6}Li scattering by ^{26}Mg [2,3].

B. Target excitation

The first step in the CC analysis of the elastic and inelastic scattering data was the inclusion of excitation to and reorientation of the first excited state of ^{26}Mg at $E_x = 1.809$ MeV using the King's College London version [16] of the Karlsruhe version [17] of the coupled-channels code JUPITOR [18,19]. The coupling strength for reorientation of the 2^+ excited state of ^{26}Mg was assumed to be equal to that for the $0^+ \leftrightarrow 2^+$ coupling. All parameters, other than the potential radii, were searched upon. The calculations assume the 0^+ and 2^+ states to be members of a ground state rotational band having $K = 0$. Coulomb corrections to the scattering were included in the calculations.

The parameter set derived from the optical model analysis of the elastic scattering was used as the starting point of a search to the differential cross-section data for scattering to the ground and first excited states of ^{26}Mg. Rusek *et al.* [2] commented that ^{26}Mg lies in a transitional region between prolate and oblate deformation. Previous analyses of inelastic scattering to the first excited state of ^{26}Mg have reported parameter sets with $\beta_2 \approx +0.3$, although some theoretical models have predicted a negative β_2 [20]. To explore the sign of β_2, searches were performed using starting values of β_2 equal to both -0.3 and $+0.3$. In both cases, the starting parameters were set 1 of Table II. The deformation parameters of the real, imaginary, and Coulomb potentials were kept equal, i.e., radial scaling was not employed. The value of β_2 for reorientation of the first excited state was set equal to that for the transition between the ground state and the first excited state. All data points were weighted equally in this search.

The parameter sets produced by the JUPITOR searches to these data are sets 2 and 3 in Table II. The cross-section predictions corresponding to these parameter sets are shown in Fig. 5; JUPITOR calculates a point every 2°, so some truncation of sharp minima and maxima is to be expected. The predictions for iT_{11} produced by these parameter sets are < 0.0001 in the angular range 0°–70° center of mass.

Radial scaling of the potential deformation parameters was also tested, the starting parameters being set 1 in Table III, and yielded the results shown in Fig. 6. The

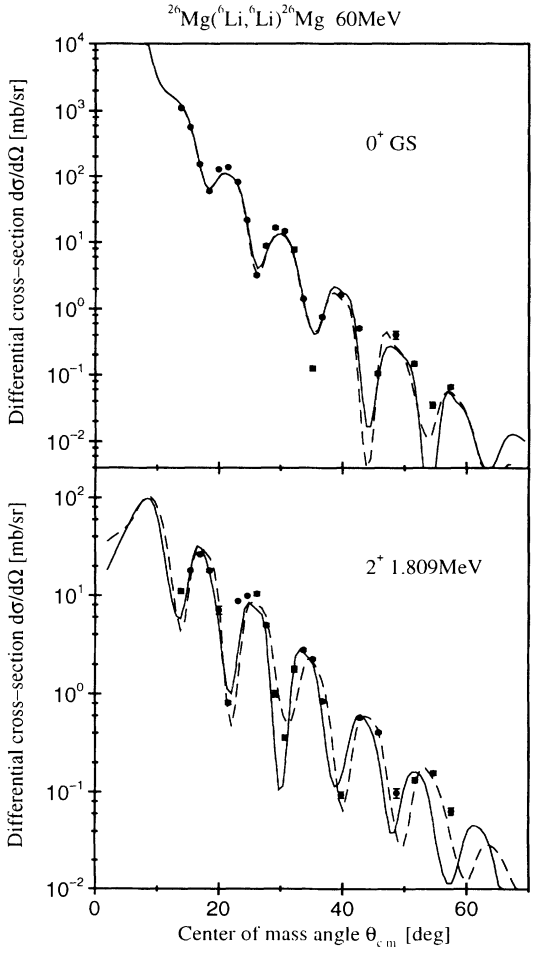

FIG. 5. CC predictions for the elastic and inelastic scattering cross sections. The solid line corresponds to positive β_2, while the dashed line corresponds to negative β_2.

TABLE III. Radially scaled deformed optical model parameters derived from the CC analysis of differential cross-section data for elastic and inelastic scattering. Potential depths are in MeV and geometric parameters are in fm.

Set	V_0	r_0	a_0	W_s	r_s	a_s	r_c	δ_2
1	166.430	1.150	0.847	15.663	2.010	0.727	1.250	±1.022
2	186.045	1.150	0.837	16.702	2.010	0.614	1.250	+1.186
3	175.659	1.150	0.847	14.928	2.010	0.646	1.250	−1.274

corresponding potential parameters, having positive and negative values of β_2, respectively, are shown as sets 2 and 3 in Table III.

Figures 5 and 6 demonstrate that calculations of the elastic scattering differential cross section are relatively insensitive to the sign of β_2. However, Figs. 5 and 6 demonstrate that the phase of the oscillations in the inelastic scattering differential cross section are best reproduced by calculations having positive β_2, especially for $\theta_{\text{c.m.}} < 50°$. Calculations with and without radial scaling of the deformation parameters yielded very similar results. The quadrupole deformation parameters deduced from this analysis are in good agreement with those deduced from light ion inelastic scattering populating the first excited state of ^{26}Mg [21,22].

C. Projectile excitation

The effects of projectile excitation and reorientation were examined using version FRV of the coupled-channels code FRESCO [23]. The ground state and unbound resonant excited states in ^{6}Li were treated equivalently, an approximation also used by Kemper *et al.* in their FRESCO analysis of the ^{12}C($^6\vec{\text{Li}}$,^{3}He)^{15}N reaction at 34 MeV [24]. This approximation has also been applied to the unbound states of ^{7}Li in analyses of $^7\vec{\text{Li}}$ scattering [25]. Hirabayashi and Sakuragi [3] demonstrated that CDCC calculations and weak-binding energy approxima-

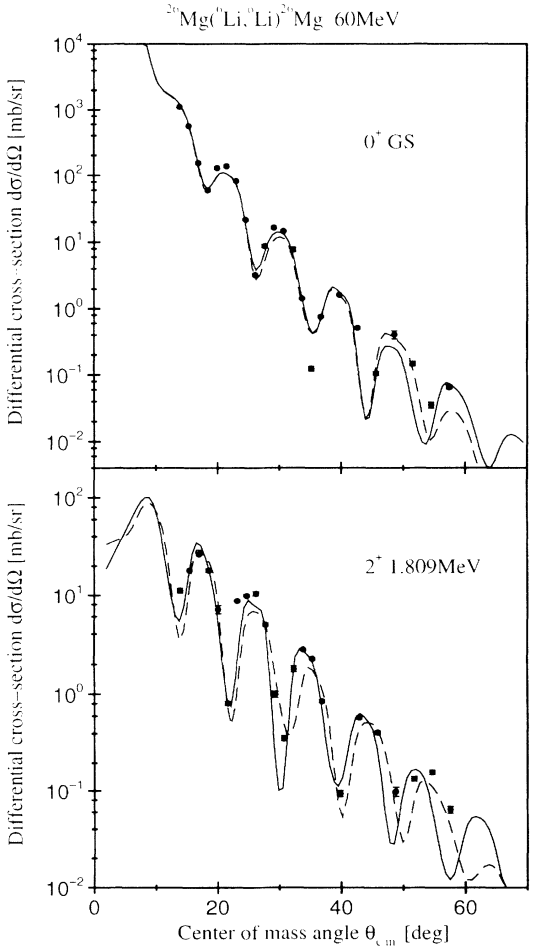

FIG. 6. Radially scaled CC predictions for the elastic and inelastic scattering cross sections. The solid line corresponds to positive β_2, while the broken line corresponds to negative β_2.

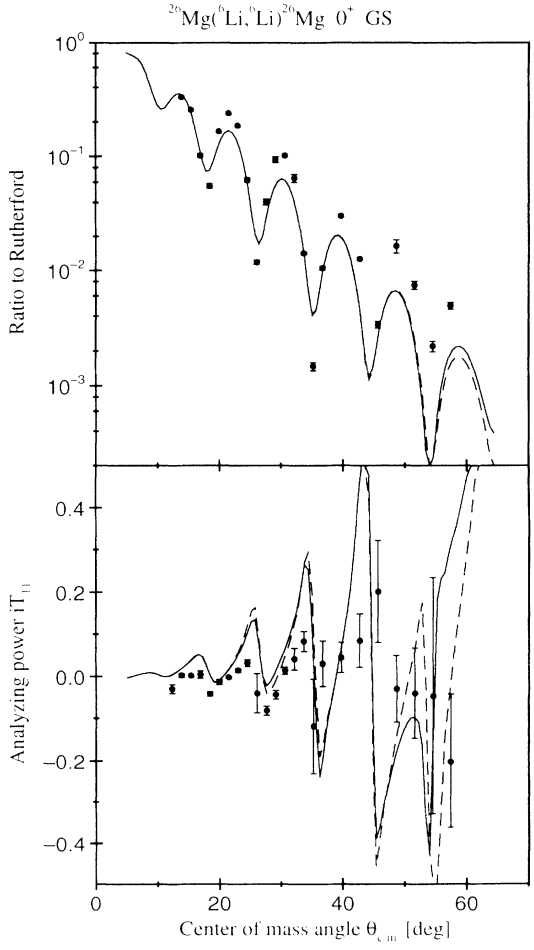

FIG. 7. Elastic scattering calculations including coupling between the $1^+_{\text{g.s.}}$ and 3^+ states of ^{6}Li. The solid line includes a static spin-orbit potential, while the dashed line neglects the static spin-orbit potential.

tion (WBEA) calculations (in which an unbound state is approximated by a weakly bound state) yield virtually identical results for $^6\vec{\text{Li}} + ^{26}$Mg elastic scattering at 44 MeV. The transition potential for the couplings was assumed to be the product of the first derivative of the potential describing the elastic scattering multiplied by a deformation length, similar to the analyses of Vineyard *et al.* [26], Van Verst *et al.* [6], and Reber *et al.* [4]. In an attempt to explore the competition between static and dynamic spin-orbit effects, otherwise identical calculations were performed with and without the static spin-orbit potential mentioned earlier.

Nuclear coupling between the ground state of ^{6}Li and the 3^+ excited state at 2.18 MeV was included with $\delta_2 = 2.19$ fm, this value being intermediate between the values of 2.34 fm and 1.89 fm deduced by Van Verst *et al.* [6] from the ^{6}Li excitation data of Vineyard *et al.* [26]. Nuclear reorientation of the 3^+ state was included with $\delta_2 = -1.10$ fm, this value being -0.5 times the deformation length for the $1^+ \leftrightarrow 3^+$ coupling. The negative sign of δ_2 for the $3^+ \leftrightarrow 3^+$ coupling was found to be necessary by Vineyard *et al.* [26]. Coulomb coupling between the 1^+ and 3^+ states was included with a strength derived from the B(E2) value between these states reported by Yen *et al.* [27]. The inclusion of these couplings generated a nonzero vector analyzing power for elastic scattering, as shown in Fig. 7. The phase of the iT_{11} data is predicted well by calculations with and without a static spin-orbit potential, but the magnitude of the oscillations is overpredicted by a factor of approximately 2. Beyond $\theta_{\text{c.m.}} \sim 60°$ both calculations predict large, positive analyzing powers.

Next, coupling was included between the ground state of ^{6}Li and the 2^+ excited state at 4.31 MeV. The strength of Coulomb coupling between these states was deduced from the B(E2) value between these states reported by Eigenbrod [28]. Nuclear coupling was included with $\delta_2 = 2.13$ fm, a value derived by Van Verst *et al.* [6] from the ^{6}Li excitation data of Vineyard *et al.* [26]. The results of calculations with these couplings are shown in

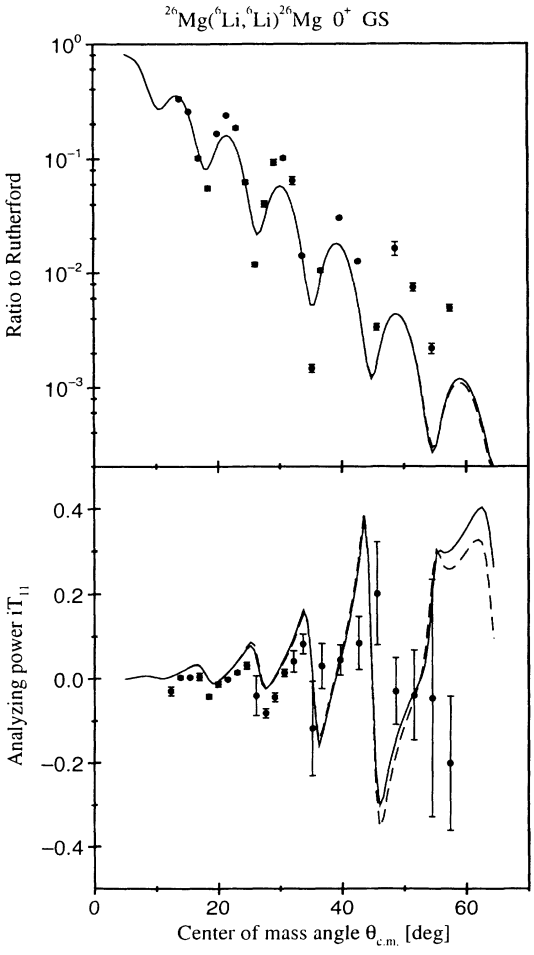

FIG. 8. Elastic scattering calculations including coupling between the $1^+_{g.s.}, 3^+$, and 2^+ states in ^{6}Li. The solid line includes a static spin-orbit potential, while the dashed line neglects the static spin-orbit potential.

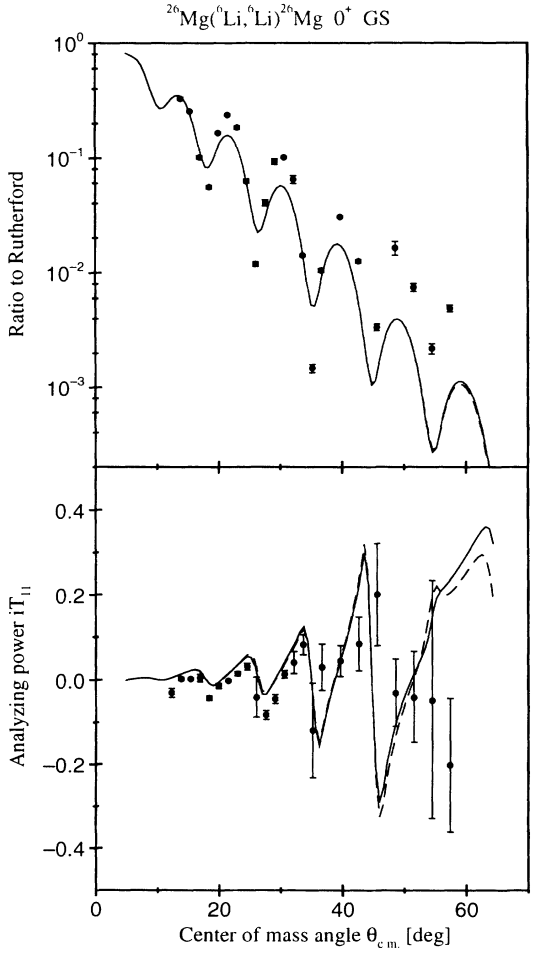

FIG. 9. Elastic scattering calculations including coupling between the $1^+_{g.s.}, 3^+, 2^+$, and 1^+ states in ^{6}Li. The solid line includes a static spin-orbit potential, while the dashed line neglects the static spin-orbit potential.

Fig. 8. Inclusion of coupling between the ground and 2^+ states of ^{6}Li has improved the description of the iT_{11} data, although a slight overprediction is manifest, and removed the prediction of large analyzing powers beyond $\theta_{c.m.} \sim 60°$.

Finally, coupling to the 1^+ state in ^{6}Li, at 5.65 MeV, was included. Coulomb coupling between the ground state and the 1^+ state at 5.65 MeV was included with the same value as for the coupling between the ground and 2^+ states, no B(E2) value having been reported for the transition between the ground and 1^+ states. No data are available for excitation of the 1^+ state in ^{6}Li, so nuclear coupling between the ground and 1^+ states was included with a deformation length $\delta_2 = 1.0$ fm, this value being approximately half that for coupling between the ground and 2^+ states. The prediction corresponding to this coupling scheme is shown in Fig. 9. With this coupling scheme, the model is able to fully describe the analyzing power data.

Figures 4, 7, 8, and 9 demonstrate that the prediction of the elastic scattering differential cross section deteriorated when inelastic effects in the projectile were included. A similar effect was observed by Kuburas *et al.* in their analysis of polarized ^{7}Li scattering using Woods-Saxon potentials [29]. To improve the present cross-section prediction, the potential parameters were modified for the full projectile excitation calculations. Figure 10 shows such a calculation using parameter set 3 in Table II. The description of the differential cross-section data in Fig. 10 is superior to that of Fig. 9, while the description of the analyzing power is largely unmodified. Parameter set 3 in Table II is almost certainly not optimal and a further improvement in the description of the differential cross-section data could almost certainly be obtained by additional modification of the interaction potential. However, this procedure was not attempted, as the necessary calculations are lengthy and FRESCO lacks an automatic grid-search facility. It is inferred from the comparison of Fig. 10 with Fig. 9 that such an improvement in the description of the differential cross-section

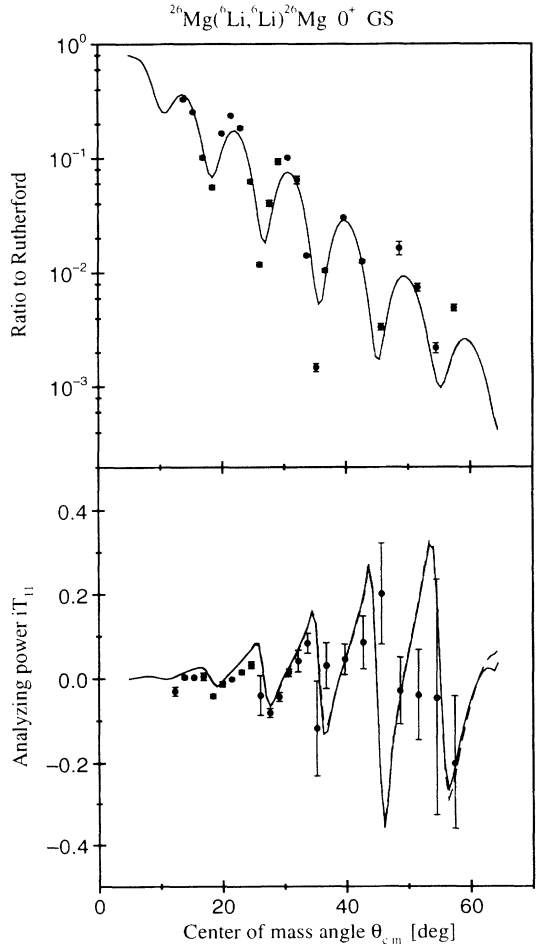

FIG. 10. Elastic scattering calculations including coupling between the $1^+_{g.s.}, 3^+, 2^+$, and 1^+ states in ^{6}Li using a modified interaction potential. The solid line includes a static spin-orbit potential, while the dashed line neglects the static spin-orbit potential.

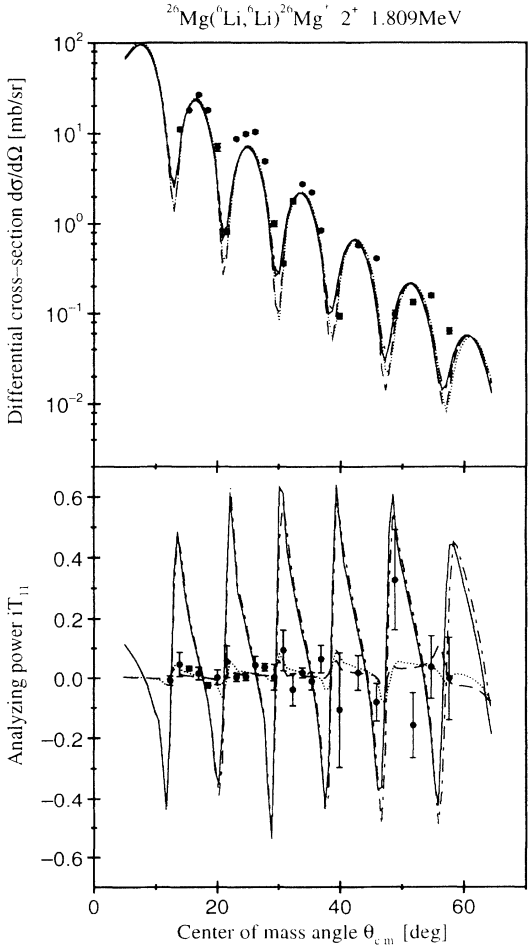

FIG. 11. CC calculations including couplings in the ^{6}Li and the ^{26}Mg. The solid line includes a static spin-orbit potential, while the dashed line neglects the static spin-orbit potential. The dot-dashed and dotted lines are the results of calculations including mutual excitation of the target and projectile, with and without a static spin-orbit potential, respectively.

data would be associated with only marginal modifications to the predicted vector analyzing powers and thus would not alter the conclusions of the analysis.

D. Target and projectile excitations

The JUPITOR analysis of differential cross-section data for elastic and inelastic scattering demonstrated that ^{26}Mg is best described as a prolate spheroid. Consequently, excitation of ^{26}Mg to the first excited state at 1.809 MeV was included with a deformation parameter $\delta_2 = 1.41$ fm, derived from set 2 in Table II using

$$\delta_2 = \beta_2 r_s A^{\frac{1}{3}} \ . \tag{4}$$

Reorientation of the excited 2^+ state was also included with $\delta_2 = 1.41$ fm. The results of calculations with this coupling scheme are shown in Fig. 11; the solid line corresponds to a calculation with a static spin-orbit potential, while the dashed line corresponds to a similar calculation without the static spin-orbit potential. The differential cross section and analyzing power data for inelastic scattering are well reproduced by the calculation without the static spin-orbit potential. However, the calculation with a static spin-orbit potential overpredicts the analyzing power data. Vector analyzing powers for inelastic scattering have been shown to be highly sensitive to the static spin-orbit potential in other analyses [4,6]. The simultaneous prediction of the elastic scattering observables obtained from this calculation differed only slightly from that shown in Fig. 10, indicating that target excitation has only a small role in the elastic scattering mechanism, in agreement with the findings of Rusek *et al.* [2]. The small magnitude of the vector analyzing power data presented in the present work places a severe constraint on the magnitude of the static spin-orbit potential for the ^{6}Li $+^{26}$ Mg system.

To explore the effects of mutual excitation, the calculations described in the above paragraph were repeated with mutual excitations to the $T = 0$ states of ^{6}Li and the first excited state of ^{26}Mg. The results of these calculations are also shown in Fig. 11, the dotted and dot-dashed lines representing calculations with and without a static spin-orbit potential, respectively. With no spin-orbit potential, slight differences are evident between calculations with and without mutual excitation. However, when a static spin-orbit potential is included, the differences between calculations with and without mutual excitation are barely discernible.

IV. CONCLUSIONS

Analysis of data for elastic and inelastic scattering has demonstrated that polarized ^{6}Li scattering at 60 MeV is similar to scattering at 44 MeV, where description of the analyzing powers was dependent upon the inclusion of couplings between the ground and excited states of the projectile. The present analysis concurs with the findings of Hirabayashi and Sakuragi [3], who concluded that to fully reproduce the analyzing power data for elastic scattering it was necessary to include couplings between the ground state of the projectile and the members of the $T = 0$ triplet at 2.18, 4.31, and 5.65 MeV. The effect of the static spin-orbit potential was found to be negligible. The calculations were extended to include inelastic scattering to the first excited state of ^{26}Mg. It was possible to reproduce the vector analyzing power for inelastic scattering without the introduction of a static spin-orbit potential, in contrast to work at 30 and 32 MeV [6,4]. However, in common with the work of Van Verst *et al.* [6] and Reber *et al.* [4], calculations of the vector analyzing power for inelastic scattering were found to be far more sensitive to the static spin-orbit potential than calculations of the vector analyzing power for elastic scattering. The results of calculations including mutual excitation of the projectile and target were found to differ only slightly from the results of inelastic scattering calculations where mutual excitation was omitted. The techniques employed in this analysis have been used to include projectile excitation effects in analyses of data for the ^{26}Mg($^6\vec{\text{Li}}$,^{6} He)^{26}Al and ^{26}Mg($^6\vec{\text{Li}}$,^{7} Li)^{25}Mg reactions [10,30].

A large body of polarized ^{6}Li scattering data is now in existence for bombarding energies between 9 MeV and 60 MeV [1]. However, many different techniques have been used in the analysis of these data, rendering the comparison of different analyses rather difficult. Thus, a consistent, global analysis of this body of data would be most welcome.

ACKNOWLEDGMENTS

This work was supported in part by the Science and Engineering Research Council of the United Kingdom under Grants GR/F/39874 (to King's College London) and GR/H/23825 (to the University of Birmingham).

[1] D. Fick, G. Grawert, and Irena M. Turkiewicz, Phys. Rep. **214**, 1 (1992).
[2] K. Rusek, J. Giroux, H.J. Jänsch, H. Vogt, K. Becker, K. Blatt, A. Gerlach, W. Korsch, H. Leucker, W. Luck, H. Reich, H.-G. Völk, and D. Fick, Nucl. Phys. **A503**, 223 (1989).
[3] Y. Hirabayashi and Y. Sakuragi, Nucl. Phys. **A536**, 375 (1992).
[4] E.L. Reber, K.W. Kemper, P.L. Kerr, A.J. Mendez, E.G. Myers, B.G. Schmidt, and V. Hnizdo, Phys. Rev. C **48**, 285 (1993).
[5] Y. Hirabayashi, Phys. Rev. C **44**, 1581 (1991).
[6] S.P. Van Verst, D.P. Sanderson, D.E. Trcka, K.W. Kemper, V. Hnizdo, B.G. Schmidt, and K.R. Chapman, Phys. Rev. C **39**, 853 (1989).
[7] E.L. Reber, K.W. Kemper, P.V. Green, P.L. Kerr, A.J. Mendez, E.G. Myers, and B.G. Schmidt, Phys. Rev. C **49**, R1 (1994).
[8] O. Karban, W.C. Hardy, K.A. Connell, S.E. Darden, C.O. Blyth, H.D. Choi, S.J. Hall, S. Roman, and G. Tun-

gate, Nucl. Instrum. Methods A **274**, 4 (1989).
[9] J.S. Lilley, Phys. Scr. **25**, 435 (1982).
[10] R.P. Ward, N.M. Clarke, C.N. Pinder, K.I. Pearce, C.O. Blyth, H.D. Choi, P.R. Dee, S. Roman, G. Tungate, and N.J. Davis, Phys. Rev. C **48**, 2366 (1993).
[11] S.E. Darden, in *Proceedings of the Third International Symposium on Polarization Phenomena in Nuclear Reactions, Madison*, 1970, edited by H.H. Barschall and W. Haeberli (University of Wisconsin Press, Madison, 1971), p. 39.
[12] N.M. Clarke, Optical model computer code HI-OPTIM 1991 (unpublished).
[13] C.B. Fulmer, G.R. Satchler, E.E. Gross, F.E. Bertrand, C.D. Goodman, D.C. Hensley, J.R. Wu, N.M. Clarke, and M.F. Steeden, Nucl. Phys. **A356**, 235 (1981).
[14] J. Cook, J.M. Barnwell, N.M. Clarke, and R.J. Griffiths, J. Phys. G **6**, 1251 (1980).
[15] G. Mairle, K.T. Knöpfle, M. Reidesel, G.J. Wagner, V. Bechtold, and L. Friedrich, Nucl. Phys. **A339**, 61 (1980).
[16] N.M. Clarke, King's College London version of the coupled-channels computer code JUPITOR, 1972 (unpublished).
[17] H. Rebel and G.W. Schweimer, Kernforschungszentrums Karlsruhe Report No. 1333, 1971.
[18] T. Tamura, Rev. Mod. Phys. **37**, 69 (1965).
[19] T. Tamura, Oak Ridge National Laboratory Report No. 4152, 1967.
[20] R.H. Spear, Phys. Rep. **73**, 369 (1981).
[21] K.I. Pearce, N.M. Clarke, R.J. Griffiths, P.J. Simmonds, D. Barker, J.B.A. England, M.C. Mannion, and C.A. Ogilvie, Nucl. Phys. **A467**, 215 (1987).
[22] P.R. Hayes, N.M. Clarke, K.I. Pearce, M.B. Becha, R.S. Mackintosh, J.B.A. England, L. Zybert, G.M. Field, and S. Roman, Nucl. Phys. **A540**, 171 (1992).
[23] I.J. Thompson, Comput. Phys. Rep. **7**, 167 (1988).
[24] K.W. Kemper, P.L. Kerr, A.J. Mendez, E.G. Myers, E.L. Reber, K. Rusek, and G. Tungate, Phys. Lett. B **321**, 183 (1994).
[25] G. Kuburas, O. Karban, C.O. Blyth, H.D. Choi, S.J. Hall, S. Roman, G. Tungate, I.M. Turkiewicz, and N.J. Davis, Nucl. Phys. **A542**, 479 (1992).
[26] M.F. Vineyard, J. Cook, and K.W. Kemper, Phys. Rev. C **31**, 879 (1985)
[27] R. Yen, L.S. Cardeman, D. Kalinsky, J.R. Legg, and C.K. Bockelman, Nucl. Phys. **A235**, 135 (1974).
[28] F. Eigenbrod, Z. Phys. **228**, 337 (1969).
[29] G. Kuburas, O. Karban, C.O. Blyth, H.D. Choi, S.J. Hall, S. Roman, G. Tungate, I.M. Turkiewicz, and N.J. Davis, Nucl. Phys. **A542**, 479 (1992).
[30] R.P. Ward, N.M. Clarke, K.I. Pearce, C.N. Pinder, C.O. Blyth, H.D. Choi, P.R. Dee, S. Roman, G. Tungate, and N.J. Davis, Phys. Rev. C (submitted).